Toxofilin upregulates the host cortical actin cytoskeleton dynamics, facilitating *Toxoplasma* invasion

Violaine Delorme-Walker[1,2,3], Marie Abrivard[2,3], Vanessa Lagal[2,3], Karen Anderson[4], Audrey Perazzi[2,3], Virginie Gonzalez[2,3], Christopher Page[4], Juliette Chauvet[2,3], Wendy Ochoa[4], Niels Volkmann[4], Dorit Hanein[4] and Isabelle Tardieux[2,3,*]

[1]Department of Immunology and Microbial Science, The Scripps Research Institute, La Jolla, CA 92037, USA
[2]Institut Cochin, Université Paris Descartes, CNRS (UMR 8104), 75014 Paris, France
[3]INSERM, U1016, 75014 Paris, France
[4]Bioinformatics and Systems Biology Program, Sanford-Burnham Medical Research Institute, La Jolla, CA 92037, USA
*Author for correspondence (isabelle.tardieux@inserm.fr)

Accepted 25 April 2012
Journal of Cell Science 125, 4333–4342

doi: 10.1242/jcs.103648

Summary

Toxoplasma gondii, a human pathogen and a model apicomplexan parasite, actively and rapidly invades host cells. To initiate invasion, the parasite induces the formation of a parasite–cell junction, and progressively propels itself through the junction, inside a newly formed vacuole that encloses the entering parasite. Little is known about how a parasite that is a few microns in diameter overcomes the host cell cortical actin barrier to achieve the remarkably rapid process of internalization (less than a few seconds). Using correlative light and electron microscopy in conjunction with electron tomography and three-dimensional image analysis we identified that toxofilin, an actin-binding protein, secreted by invading parasites correlates with localized sites of disassembly of the host cell actin meshwork. Moreover, quantitative fluorescence speckle microscopy of cells expressing toxofilin showed that toxofilin regulates actin filament disassembly and turnover. Furthermore, *Toxoplasma* tachyzoites lacking toxofilin, were found to be impaired in cortical actin disassembly and exhibited delayed invasion kinetics. We propose that toxofilin locally upregulates actin turnover thus increasing depolymerization events at the site of entry that in turn loosens the local host cell actin meshwork, facilitating parasite internalization and vacuole folding.

Key words: *Toxoplasma*, Toxofilin, Actin dynamics, Cofilin, Host cell invasion, Electron tomography, Speckle fluorescent microscopy

Introduction

The protozoan parasite *Toxoplasma gondii*, which belongs to the phylum Apicomplexa, causes toxoplasmosis in animals and humans. Although usually mild, this disease can become severe to lethal when parasite multiplication is uncontrolled as in immunocompromised patients and in fetuses of primoinfected mothers. *Toxoplasma* multiplies in host cells as tachyzoites, inside a sub-cellular compartment called the parasitophorous vacuole (PV). Formed during the remarkably rapid invasion process that lasts a few seconds, the PV largely derives from the host plasma membrane (PM) bilayer that invaginates around the entering parasite and eventually pinches off from the PM by membrane fission (Suss-Toby et al., 1996). The PM starts to fold inward when the parasite triggers the assembly of a unique zoite–cell junction, herein called a tight junction (TJ). Recent studies have highlighted the major contribution of a complex of RON proteins, located in the thin neck of the rhoptries, in building up the TJ (Alexander et al., 2005; Straub et al., 2009; Besteiro et al., 2009).

Although the TJ is thought to serve as a molecular sieve preventing most host proteins enter the nascent PV (Mordue et al., 1999), it also ensures the active propelling of the zoite into the cell. Indeed, the driving force generated by the parasite actomyosin motor (Dobrowolski and Sibley, 1996; Meissner et al., 2002) is exerted onto a stable TJ anchored to the host cytoskeleton through de novo host cell actin polymerization (Gonzalez et al., 2009). However, given the 1.5-2.5 μm diameter of the parasite, the formation of the PV that surrounds the parasite and internalization of the tachyzoite into the host cell are expected to require local loosening of the host cortical actin network.

Toxofilin is an actin-binding protein isolated from *Toxoplasma gondii*. *In vitro*, this 27-kDa protein binds to both mammalian and parasite actin and regulates actin dynamics through monomer sequestration and barbed-end filament capping (Poupel et al., 2000). A 14-kDa domain of toxofilin, spanning amino acids 69-196, carries both activities (Jan et al., 2007). Analysis of the atomic structure of the toxofilin$_{69\text{-}196}$–G-actin complex revealed that toxofilin, which is made up of five helices, binds to the actin nucleotide at residue Gln134 in helix 4, and that one toxofilin molecule interacts with two actin molecules organized as an antiparallel dimer. Although toxofilin appears to be a potent actin nucleotide-exchange inhibitor (Lee et al., 2007), its function *in vivo* remains undefined.

Toxofilin has an N-terminal signal sequence for secretion and has been found predominantly in apical pear-shaped secretory vesicles called rhoptries (Bradley et al., 2005), which play a crucial role in invasion by releasing their contents inside the host cell. The presence of toxofilin inside host cells was ascertained

by a FRET-based β-lactamase assay (Lodoen et al., 2010). Nevertheless, the location and function of toxofilin during invasion remain elusive.

In this study, we investigated the possibility that toxofilin is secreted into the host cell cytoplasm where it targets the host cortical actin cytoskeleton to facilitate the proper vacuole folding and thus the invasion process. We first demonstrate that tachyzoites lacking toxofilin are impaired in cortical actin disassembly and have a dynamic behavior during cell entry that is strikingly different from that of normal tachyzoites. Using correlative light and electron microscopy combined with electron tomography, followed by three-dimensional (3D) analysis, we also show that toxofilin secreted by invading tachyzoites specifically associates with the loosened host actin meshwork. Moreover, using an actin barbed-end assay and quantitative fluorescent speckle microscopy (qFSM) to measure actin filament (F-actin) dynamics, we provide evidence that toxofilin facilitates tachyzoite invasion by regulating host cortical actin filament turnover.

Results

Toxofilin knockout tachyzoites display a defective invasive behavior

Recently, toxofilin knockout (KO) *T. gondii* tachyzoites were reported to be capable of invading host cells, when measured by counting the number of intracellular parasites relative to the total number of parasites after 30- to 180-second invasion assays (Loeden et al., 2010). To search for defects in cell invasion by KO tachyzoites that might not impact the overall invasion efficiency but still provide information on toxofilin function, we used videomicroscopy to analyze the dynamics of entry of wild-type (WT) and toxofilin-KO parasites in fibroblast and epithelial cells (Fig. 1A-C). WT tachyzoites typically entered cells by smoothly sliding through a junction. A constriction moved down the tachyzoite as it passed through the entering point. The constriction was typically about a third of the width of the tachyzoite section and thus was readily visible by videomicroscopy (Fig. 1A, black arrows; supplementary material Movie 1). Interestingly, quantification of the constriction size derived from movie analysis showed that the toxofilin-KO sample had a significantly tighter TJs (Fig. 1B,D, black arrows; supplementary material Movie 2). Indeed, ~46% of toxofilin-KO tachyzoites invading cells had unusual kinks and twists, as if disturbed by a local tension impeding smooth penetration (Fig. 1B, arrowheads; supplementary material Movie 3). These unusual kinks and twisted entries were not observed for WT tachyzoites. The percentage of abnormal behaviors increased to 72% when human foreskin fibroblasts (HFF) cells were confluent. In non-confluent HeLa cells, ~37% of the invading toxofilin-KO tachyzoites stopped their forward progression, reoriented and pulled the host cell plasma membrane around them while remaining extracellular (supplementary material Movie 3), again a behavior not observed for WT tachyzoites. Lastly, 8.2% of toxofilin-KO tachyzoites remained immobilized for several minutes during invasion before eventually disengaging from the refractory cell. From the first evidence of parasite constriction to the final mark of constriction at the posterior end, the invasion process lasted 17.4±7.07 seconds for the WT tachyzoites (Fig. 1A,C; supplementary material Movie 1). In contrast, the average time of internalization by toxofilin-KO tachyzoites was significantly increased to 33.1±19.1 seconds and reached 60.1±16.9 seconds when only atypical behaviors of entry were analyzed (Fig. 1B,C). Taken together, these data indicate that toxofilin-KO tachyzoites display a defective invasive behavior.

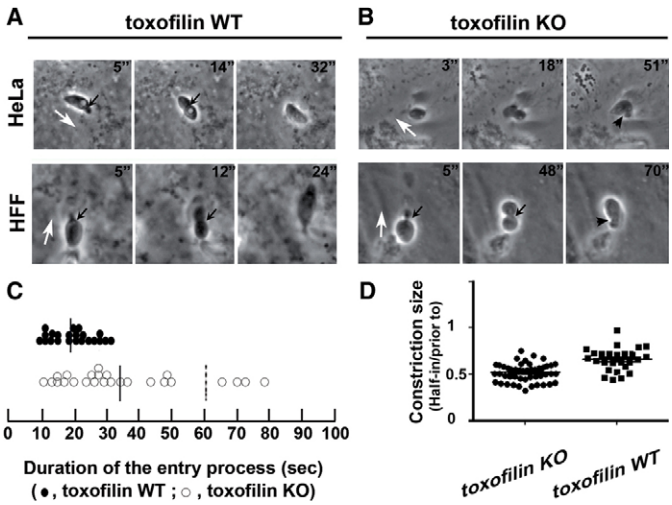

Fig. 1. Toxofilin knockout (KO) tachyzoites display atypical invasive behaviors. (**A**,**B**) Time-lapse images of invasion events by (A) toxofilin WT and (B) toxofilin-KO tachyzoites in HeLa (upper lane) and HFF cells (lower lane). The forward movement into the cell is indicated with white arrows. Parasite constriction during the invasion process is indicated by black arrows (n=40 and 49 cells for WT and KO parasites, respectively). (**C**) Graph representing the duration of the entry process in HeLa cells (n=22 and 25 invasion events for WT and KO parasites respectively; P<0.05, Student's t-test). Black straight lines represent the average entry time for both populations, and the dashed black line indicates the average time for entry of atypical invasion by KO tachyzoites. (**D**) Graph representing the size of the constriction of WT (n=30) and KO (n=46) parasites (P<0.05, Student's t-test).

Toxofilin-KO tachyzoites do not associate with disassembled cortical actin network

Since toxofilin is an actin-binding protein with monomer sequestering and barbed-end binding capabilities *in vitro* and since the video-recording of invasion by toxofilin-KO tachyzoites suggested toxofilin plays a role during the invasion process, we next investigated whether toxofilin could affect the host actin network morphology during invasion. Using traditional fluorescence microscopy, we could distinguish a local disorganization of the host F-actin cytoskeleton at the site of entry together with an already described accumulation of actin at the PV and at the cell–zoite junction (supplementary material Fig. S1A). However, the limited resolution of the approach precluded conclusions about the morphology of the host cell actin network. To achieve higher resolution, we used electron microscopy and compared the host cortical actin cytoskeleton at sites of entry by toxofilin-KO and WT parasites. To this end, we optimized the detection of invading tachyzoites and of the host cell network at the site of entry, by applying a correlative assay based on a combination of fluorescent microscopy and various electron microscopy imaging approaches: correlative light and electron microcopy (CLEM). To allow correlation between the various resolution imaging techniques, Ptk1 epithelial cells were grown in cell culture dishes on substrates amenable for both high-resolution light and electron microscopy imaging (see Materials and Methods). The major surface-exposed protein of the parasite (P30) that is not found on the host cell was used as a spatial marker for the progression on invasion.

Phase-contrast and fluorescence microscopy were employed to discriminate between non-internalized (P30 fully positive), fully internalized (P30 fully negative) and actively invading tachyzoites (P30 positive for the extracellular rear part of the parasite and P30 negative for the intracellular apical region; Fig. 2A,G; supplementary material Fig. S1B). As P30 is surface exposed, antibody labeling would not require cell permeabilization. Guided by phase-contrast and fluorescence information, we were able then to image the same tachyzoites using electron microscopy to characterize, at higher resolution, the actin morphology of the host cell at the site of entry.

We previously published the characteristic morphology of the actin cytoskeleton network in Ptk1 cell lines. Using correlative quantitative fluorescence microscopy and electron microscopy (qFSM/EM) we were able to identify a dense and continuous actin network, which extends ~15 µm from the PM towards the cell cytoplasm (Gupton et al., 2005; Delorme et al., 2007). In contrast to these previous observations, toxofilin WT tachyzoites identified at the onset of the cell invasion process (Fig. 2A-G) could be seen associated with local loosened areas of the host actin cytoskeleton (Fig. 2B,C,E,F). As invasion proceeded, dissolution of the host actin cytoskeleton progressively extended around the intracellular apical region (19 invading tachyzoites were examined; Fig. 2G–I). Within less than 6 minutes after internalization, the host actin cytoskeleton surrounding the PV that contained the parasite appeared normal (supplementary material Fig. S1B–D). All the controls for specificity of the immunolabelings are shown in supplementary material Fig. S2. To further analyze the details of the host cell actin network at sites of tachyzoite entry, we employed electron tomography and 3D image analysis. The reconstructed 3D volumes of the imaged assemblies captured in the cell environment (Hanein, 2010), allowed faithful representation of the actin network surrounding the invading parasite. The 3D reconstruction (Fig. 2J–N; supplementary material Movie 4) confirmed the absence of the actin cytoskeleton in the apical region of invading tachyzoites. In sharp contrast, no network disassembly was observed during entry of toxofilin-KO parasites, which were found to be surrounded by a well-preserved actin cytoskeleton network (eight invading KO tachyzoites were examined; Fig. 3A-G). Together, these data suggest that toxofilin facilitates tachyzoite penetration into the host cell by locally dispersing the host cell cortical actin barrier.

Apart from toxofilin, invading tachyzoites secrete other rhoptry products, some of which form vesicles called evacuoles, which have been hypothesized to contribute to the new PV compartment (Håkansson et al., 1999). Therefore, we investigated whether the lack of toxofilin could interfere with the process of evacuole secretion and possibly the host cell cortical network organization. We observed that the number of tachyzoites secreting Rhop1-positive evacuoles was not significantly different between toxofilin WT and KO parasites (33±8% and 28±7%, respectively; $P>0.05$, $n=100$). As illustrated in Fig. 3H-O, these results indicate that the rhoptry discharge in toxofilin- KO parasites is still efficient and thus the absence of host cell network disorganization observed during toxofilin- KO tachyzoite invasion is likely not to be due to a defect in evacuole secretion.

Toxofilin targets the host cell cortical actin network during invasion

To investigate whether toxofilin could regulate the host cell cortical actin, we examined its localization in tachyzoites. It had

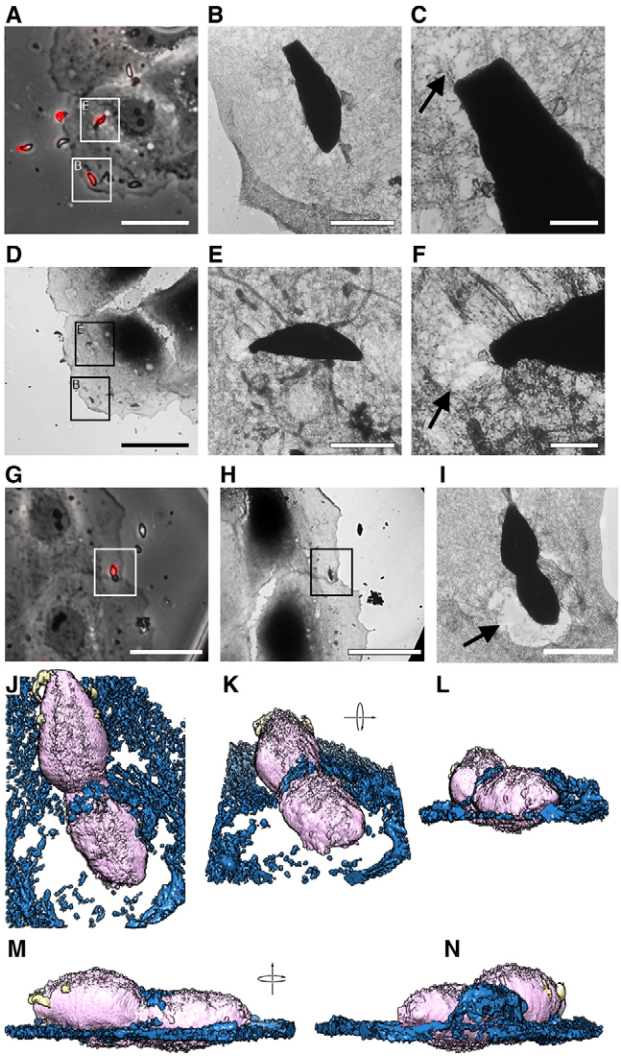

Fig. 2. Tachyzoites are associated with sparse cortical actin network upon PtK1 cell entry. (**A**) Overlay of P30 fluorescence image (red) and a phase-contrast microscopy image of invading toxofilin WT parasites. Scale bar: 30 µm. (**D**) Transmission electron micrograph of the same field of view at the same magnification as shown in A. (**B**,**E**) High resolution electron micrographs of non-internalized tachyzoites identified by P30 fluorescence in A. Scale bars: 2 µm. (**C**,**F**) Enlarged image of the tachyzoites in B and E. Note the extent of cytoskeleton loosening (black arrow). Scale bars: 500 nm. (**G**) Overlay of P30 fluorescence image (red) and phase-contrast microscopy image. (**H**) Transmission electron micrograph of the same field of view at the same magnification as shown in G. Scale bars: 30 µm (G,H). (**I**) High resolution electron micrograph of the tachyzoite marked in G and H. Note the large area devoid of cytoskeleton at the apical (black arrow), non-fluorescing part of the tachyzoite. Scale bar: 2 µm; $n=19$ invading tachyzoites. (**J-N**) Surface representation of the tomogram depicting the same tachyzoite (pink and yellow) shown in G-I. See also supplementary material Movie 1. The material associated with the host cell is shown in blue. The view in K is rotated by 60° around the indicated axis with respect to the view in G-J. The view in L is rotated by 90° with respect to the view in G-I and represents a view parallel to the plasma membrane of the host cell. (**M**,**N**) Two views rotated by 60° anti-clockwise and clockwise respectively, relative to the view shown in L, around the indicated axis. In I-K the lack of host actin cytoskeleton around the invading tachyzoite is apparent.

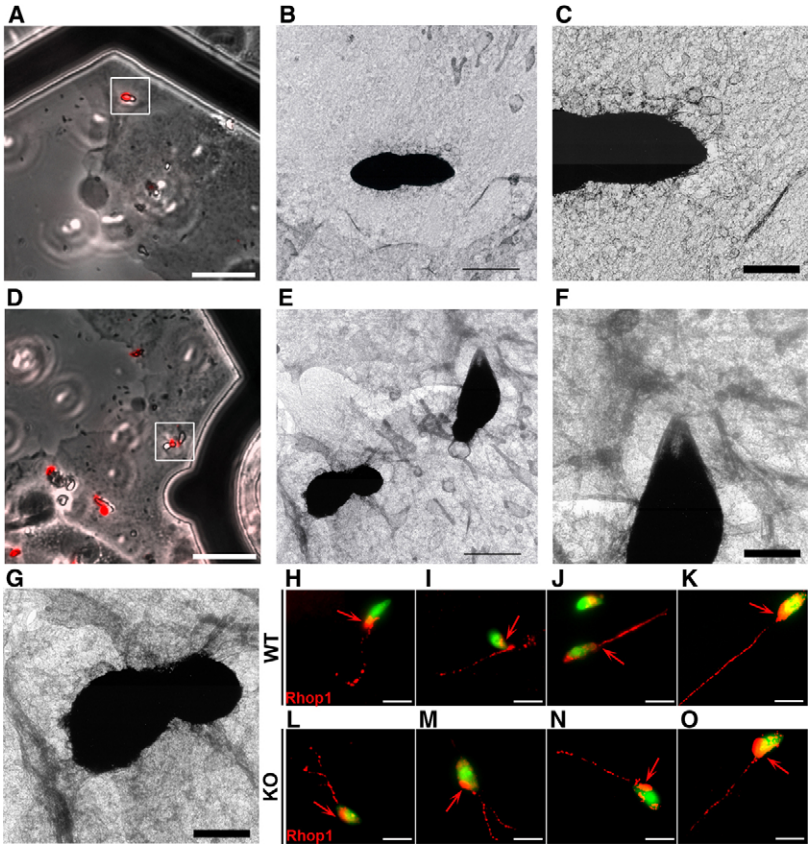

Fig. 3. Toxofilin knockout (KO) tachyzoites are not associated with a sparse cortical actin network upon entry into PtK1 cells and they are able to secrete evacuoles. (**A**,**D**) Overlay of P30 fluorescence image (red) and a phase contrast microscopy image of invading toxofilin-KO parasites. Scale bars: 20 μm. (**B**,**E**) High resolution electron micrograph of invading tachyzoite identified by P30 fluorescence in A and D. Scale bars: 2 μm. (**C**,**F**,**G**) Enlarged images of the tachyzoites in A and D. Scale bars: 1 μm. Note the integrity of the host cell cytoskeleton surrounding the invading tachyzoite beyond the constriction (n=8 invading tachyzoites). (**H-O**) Rhop1 fluorescent labeling of evacuoles (red) secreted by toxofilin WT (H-K) and KO (L-O) tachyzoites expressing GFP in HFF confluent cells. Red arrows point to the rhoptry. Scale bars: 5 μm.

been shown previously that in intracellular parasites His-tagged toxofilin was present in the rhoptry bodies possibly extending into the neck region (Bradley et al., 2005). We stained the endogenous toxofilin using anti-toxofilin antibodies and observed that toxofilin was in both the rhoptry bulb and the Ron4-positive neck compartment (Fig. 4A-D, arrows). Toxofilin was clearly detected within the elongated structure/neck region in extracellular tachyzoites treated with the actin-stabilizing drug jasplakinolide, which is known to induce a membrane-enclosed apical projection supported by newly formed actin filaments (Shaw and Tilney, 1999) (Fig. 4E, arrows). Together, these immunostainings suggest that, similar to the RON proteins, toxofilin might be delivered into the host cell early during invasion.

To investigate whether toxofilin is secreted and localizes within the entry sites, we then performed immunogold labeling in conjunction with electron tomography. The preservation of the cell cytoskeleton ultrastructure at high resolution using our protocols has been previously established (Delorme et al., 2007), suggesting the conservation of the cytoskeleton antigenicity, 3D structure and components. We focused on tachyzoites at early stages of host cell invasion when cortical actin needs to be dispersed for the parasite to enter (Fig. 5; supplementary material Movies 5, 6). The concentration of immunogold labels within a 5 μm radius of invading tachyzoites was 0.12 ± 0.06 labels/μm^2 as compared to 0.03 ± 0.03 labels/μm^2 in randomly selected host cell regions far removed from invading tachyzoites, a difference highly statistically significant at $P<0.00005$. Therefore, we concluded that toxofilin was consistently localized in close association with invading tachyzoites. As described in Fig. 2, we observed dissolution of the cytoskeleton at the entry site that was in contrast to the pristine preservation of the cytoskeleton in other regions of the host cell. Interestingly, the toxofilin labels were preferentially found in regions where the actin cytoskeleton was sparse (Fig. 5). Although toxofilin was first detected in the vicinity of the host cell surface, it was then detected deeper inside the host cell, concurrent with the proceeding invasion (Fig. 5F-J, compare E and J). The secreted toxofilin remained closely associated with the tachyzoite entry site (supplementary material Fig. S3), supporting the notion that toxofilin is locally secreted into the host cell early on during entry.

Toxofilin regulates F-actin kinematics and kinetics in living cells

Our data indicate that toxofilin is secreted into host cells during parasite entry and associates with the local loosened host actin cytoskeleton meshwork. This suggests that toxofilin has a role in regulating host cell F-actin dynamics during toxoplasma invasion. qFSM analysis provides detailed spatiotemporal maps of the velocity of F-actin flow (kinematics) and of the organization of F-actin assembly and disassembly (kinetics) in live cells (Waterman-Storer et al., 1998; Danuser and Waterman-Storer, 2006), and thus can serve as a powerful technique for investigating the regulatory role of toxofilin in living cells. Here we employed qFSM of PtK1 cells microinjected with X-rhodamine actin and expressing various toxofilin constructs to further reveal the regulatory role of toxofilin.

In migrating control cells, actin filaments are organized in two distinct structures at the leading edge: the lamellipodium, which resides at the cell edge, and the lamella, which extends from near

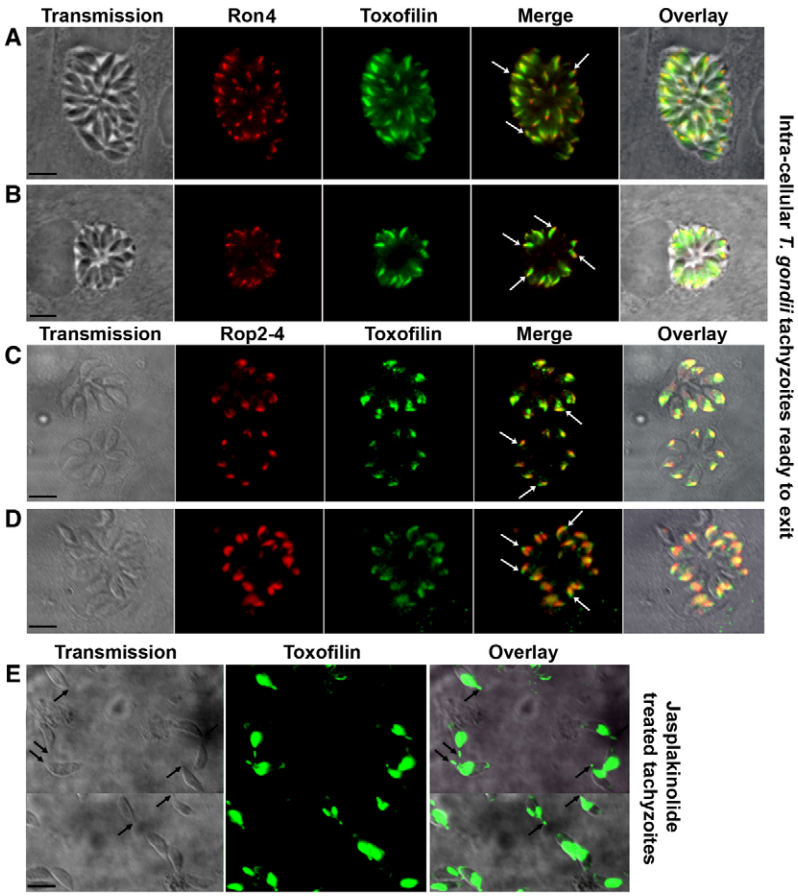

Fig. 4. Toxofilin localizes to the bulb and the neck of the rhoptry secretory vesicles. (**A-D**) Immunofluorescence of HFF cells infected with *T. gondii* tachyzoites for ~24 h. Samples were stained for (A,B) the rhoptry neck protein Ron4 (red) and toxofilin (green), or (C,D) the Rhop2-4 proteins (red) and toxofilin (green). Arrows indicate the apical neck localization of toxofilin. (**E**) Jasplakinolide-treated tachyzoites. Arrows mark the presence of toxofilin in the membrane-enclosed apical projections. Scale bars: 10 μm.

the cell edge to ~15 μm toward the cell interior (Ponti et al., 2004) (Fig. 6A–D, upper row). F-actin nucleates and polymerizes into a dense filament network at the leading edge and moves rearward through the protrusion by a process referred to as retrograde flow, which involves F-actin severing and/or disassembly. Fast actin retrograde flow, rapid F-actin polymerization (Fig. 6E, top row, bright red punctae) and subsequent depolymerization (Fig. 6E, top row, bright green punctae) are the signatures of the lamellipodium fast treadmilling network, whereas the lamella is marked by a slow retrograde flow (Fig. 6C,D) and is characterized by random foci of weaker actin polymerization and depolymerization (Fig. 6E). In contrast to control cells, cells expressing low levels of WT toxofilin or toxofilin$_{69\text{-}196}$ displayed only one region of F-actin kinematics at the cell edge (Fig. 6A–D, two bottom rows). qFSM and kymograph analysis revealed that this region exhibited a significantly faster F-actin retrograde flow compared to control cells, not only at the leading edge (Fig. 6F) but throughout the entire protrusion (Fig. 6G). Furthermore, expression of full-length WT toxofilin or toxofilin$_{69\text{-}196}$ induced the polymerization band to extend farther into the protrusion, and mainly depolymerization events occurred in the cell area behind the wide F-actin assembly band (Fig. 6E). Interestingly, this phenotype of F-actin kinetics and kinematics was similar to that already described in PtK1 cells expressing activated cofilin (Delorme et al., 2007), thus suggesting that toxofilin could sever actin filaments in addition to its known activities of F-actin capping and monomer sequestering.

We previously reported that toxofilin activity on actin was regulated by phosphorylation of toxofilin serine 53 (S53) *in vitro* and probably *in vivo* (Delorme et al., 2003) (supplementary material Fig. S4). We thus investigated the effect of S53 phosphorylation status on F-actin dynamics in living cells using FSM. Whereas expression of a non-phosphorylatable toxofilin mutant (toxofilin S53A) did not affect F-actin kinetics and kinematics (Fig. 7, bottom row), expression of a phosphomimetic toxofilin mutant (toxofilin S53E) reproduced the effects observed with WT toxofilin and toxofilin$_{69\text{-}196}$ (Fig. 7, top row). Indeed, activated toxofilin S53E significantly increased F-actin retrograde flow rates throughout the entire protrusion (Fig. 7F,G) and induced the formation of a fast treadmilling network at the leading edge (Fig. 7E). Taken together, these results indicate that toxofilin can spatially and temporally regulate F-actin dynamics in living cells when phosphorylated on S53.

Toxofilin increases local free barbed filament ends at the cell edge

The striking effect of toxofilin in enhancing actin filament dynamics and turnover in Ptk1 cells prompted us to test whether toxofilin could affect the distribution and density of polymerization-competent free barbed-ends, as we had previously observed for cofilin (Delorme et al., 2007). In control cells, free barbed-ends were localized in a narrow rim along the leading edge (Fig. 8A). In cells expressing toxofilin WT, toxofilin$_{69\text{-}196}$ or active toxofilin S53E, actin incorporation at free barbed-ends was dramatically increased (Fig. 8B–D, respectively). Expression of a

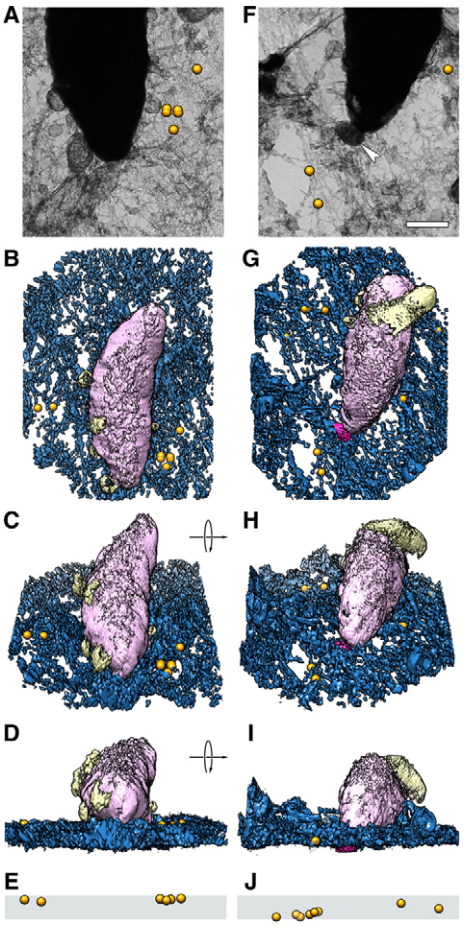

Fig. 5. Gold-labeled toxofilin localizes at the site of tachyzoite invasion. (**A**,**F**) Electron micrograph of non-internalized tachyzoites with gold labels (toxofilin) shown as orange spheres. Scale bar: 500 nm. A larger field of view is shown in supplementary material Fig. S3. White arrowhead in F indicates the apex of the entering parasite. (**B-D**,**G-I**) Surface representations of the tomograms of the same tachyzoites shown in a and f. See also supplementary material Movies 5 and 6. C and H are rotated 60° with respect to the corresponding view in A,B and F,G, respectively, around the indicated axis. D and I are rotated by 90°, representing a view parallel to the host cell plasma membrane. The tachyzoite is shown in pink and yellow, the host cell material (membrane and cytoskeleton) in blue. (**E**,**J**) Individual labels from the views in D and I, respectively, mapped onto the thickness of the host cell (symbolized as a gray box; $n=17$ invading tachyzoites).

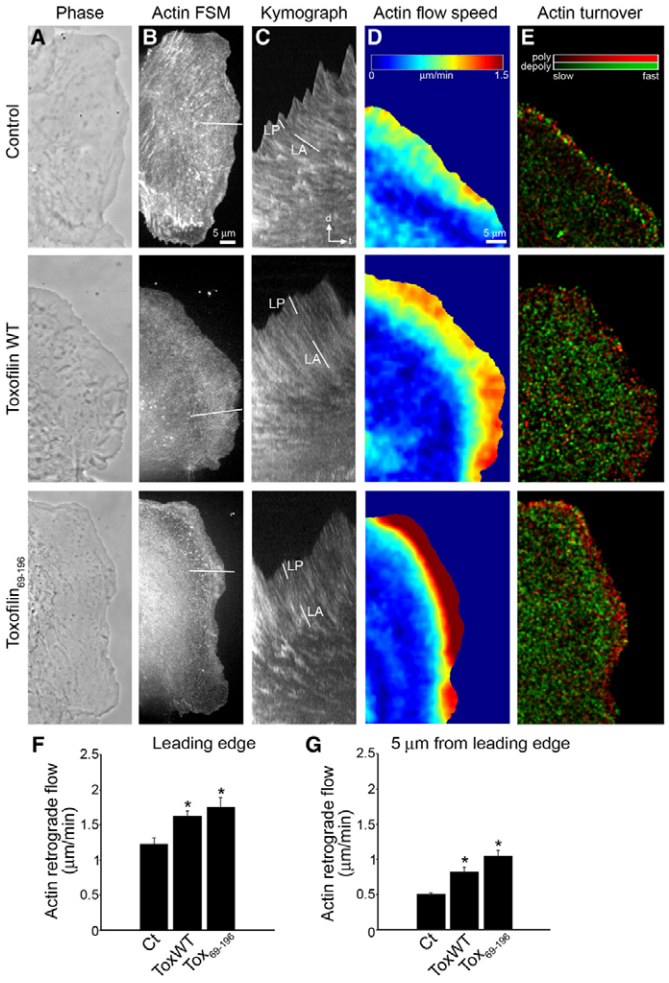

Fig. 6. Toxofilin expression increases F-actin flow and treadmilling. (**A**,**B**) Phase-contrast (A) and FSM images of X-rhodamine actin (B) in motile PtK1 cells expressing GFP (control), GFP–toxofilin WT or GFP–toxofilin$_{69\text{-}196}$. Scale bar: 5 µm. (**C**) Kymographs taken along the axis of F-actin flow (indicated by a line in B). The lines indicate the positions where the F-actin flow rates were measured in the lamellipodium (LP) and lamella (LA). Time bar (t), 2 min; scale bar (d), 2 µm. (**D**) qFSM kinematic maps of the speed of F-actin flow. Note the faster flow (red) in cells expressing toxofilin. Scale bar: 5 µm. (**E**) qFSM kinetic map of F-actin polymerization (red) and depolymerization (green) rates. Brightness indicates relative rate magnitude. (**F**,**G**) Average rates of F-actin retrograde flow in the lamellipodium (F) and the lamella (G) of cells expressing GFP (Ct), GFP–toxofilin WT (ToxWT), GFP–toxofilin$_{69\text{-}196}$ (Tox$_{69\text{-}196}$). Values are means ± s.e.m. Toxofilin expression significantly increased F-actin flow rates at the cell edge. *$P<0.001$ versus control cells, Student's t-test. $n\geq18$ cells for each condition, with a minimum of 450 measurements per condition.

non-phosphorylatable toxofilin S53A mutant did not affect free barbed-end density (Fig. 8E). These observations were confirmed by quantification of the ratio of barbed-end fluorescence intensity to F-actin intensity (Fig. 8F–H): whereas free barbed-ends localized in a 1 µm wide band in control (black) and toxofilin S53A-expressing cells (blue), this band widened to 2 µm upon expression of toxofilin WT (red), toxofilin$_{69\text{-}196}$ (pink) or toxofilin S53E (green). Furthermore, polymerization-competent free barbed-end density was also enhanced, with a maximum intensity ratio of 4.01, 3.75 and 3.48 in cells expressing toxofilin WT, toxofilin$_{69\text{-}196}$ and toxofilin S53E, respectively, compared to a maximum of 2.1 and 1.98 in control cells and cells expressing toxofilin S53A, respectively. This phenotype, again, is similar to the increased width of the actin treadmilling array and density of free barbed-ends we previously observed in cells expressing activated cofilin (Delorme et al., 2007). Interestingly, all GFP–toxofilin constructs, but not the GFP vector control, were localized at the cell leading edge after cell permeabilization during the free barbed-end assay. This observation confirms the interaction of toxofilin with the lamellipodium actin network and reinforces the notion of functional similarities to cofilin.

Toxofilin upregulates actin turnover independently of host cell cofilin

The 3D structure of the toxofilin$_{69\text{-}196}$–actin complex revealed that toxofilin helix 4 fits in a cleft in actin subdomain 4 that is fully

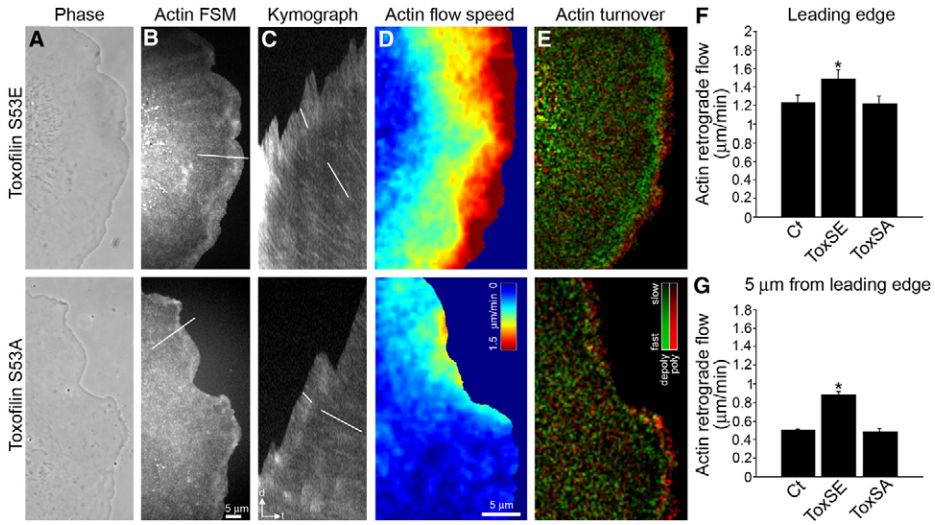

Fig. 7. Phosphorylation of toxofilin on serine 53 regulates its activity on F-actin dynamics. (**A**,**B**) Phase-contrast (A) and FSM images of X-rhodamine actin (B) in motile PtK1 cells expressing GFP–toxofilin S53E or GFP–toxofilin S53A mutants. Scale bar: 5 µm. (**C**) Kymographs taken from lines oriented along the axis of F-actin flow (indicated in B). Lines in C indicate the positions where the F-actin flow rates were measured in the lamellipodium (upper) and lamella (lower). Time bar (t), 2 min; scale bar (d): 2 µm. (**D**) qFSM kinematic maps of the speed of F-actin flow. (**E**) qFSM kinetic map of F-actin polymerization (red) and depolymerization (green) rates. Brightness indicates relative rate magnitude. Scale bar: 5 µm. (**F**,**G**) Average rates of F-actin retrograde flow in the lamellipodium (F) and the lamella (G) of cells expressing GFP (Ct), GFP–toxofilin S53E (ToxSE) or GFP–toxofilin S53A (ToxSA). Values are means ± s.e.m. Phosphomimetic toxofilin mutant expression significantly increased F-actin flow rates and turnover at the cell edge. *$P<0.001$ versus control cells, Student's *t*-test. $n\geq18$ cells for each condition, with a minimum of 450 measurements per condition.

exposed in the actin filament (Lee et al., 2007). Because the highly conserved Ras-GAP family member Aip1 has a binding site that has been mapped to this cleft and cooperates with cofilin to regulate actin turnover (Rodal et al., 1999; Ono, 2003), we checked whether toxofilin could similarly act by cooperating with cofilin/actin depolymerizing factor (ADF) in the host cells. To this end, we tested whether toxofilin could associate with cofilin. We performed tag-affinity pull down of toxofilin from extracts of HEK293 cells expressing either myc–toxofilin alone or in combination with hemagglutinin (HA)–cofilin. Neither endogenous cofilin nor the abundant tubulin was found associated with myc–toxofilin immunoprecipitates whereas actin was co-precipitated as expected (supplementary material Fig. S5A). In cells expressing both myc–toxofilin and HA–cofilin, myc–toxofilin immunoprecipitation did not trap HA–cofilin (supplementary material Fig. S5B). Consistently, when HA–cofilin was pulled down, no myc–toxofilin was found in cofilin-containing eluates (data not shown). These data indicate that toxofilin and cofilin are not interacting with each other despite their relative abundance in the transfected cells, which indicates that toxofilin activity is not induced or synergized by the host cell cofilin. Consistently, invasion assays using HeLa cells showed that control and cofilin-silenced cells are equally permissive to *T. gondii* (supplementary material Fig. S5C,D).

Discussion

In order to adhere to or invade cells, microorganisms commonly subvert host cell properties to induce local remodeling of the cell plasma membrane in a process tightly coupled to cortical actin dynamics. These events can be spectacular as, for example, during attachment of pedestal-forming bacteria (EPEC) to host cells (Vallance and Finlay, 2000) or during the phagocytic engulfment of invasive bacteria (*Shigella* and *Salmonella*) (Tran Van Nhieu et al., 2000). They can also be more discrete, such as during the particularly rapid internalization of apicomplexan parasites (tens of seconds). Most apicomplexan parasites activate their own actomyosin-based motor to generate forward motion into a nascent PV. Although the internalization process has long been thought to occur independently of changes in the host cytoskeleton (Bradley and Sibley, 2007), it was shown recently that host cell actin filament assembly at the TJ is necessary for proper zoite internalization (Gonzalez et al., 2009) to anchor the TJ to the cell cytoskeleton. In addition, the formation of a new sub-cellular compartment of about 15-20 µm^3 from the PM and the progression of the parasite inside the cell probably requires local loosening of the cortical actin barrier. Of note, when host cells are pretreated with jasplakinolide, which stabilizes actin filaments, they become refractory to subsequent parasite entry (Gonzalez et al., 2009), which is consistent with a need for host cortical actin filament dissolution during invasion. The molecules responsible for this local host actin remodeling could originate either from the host cell, and be possibly activated by parasite products, or from the parasite itself. In this study, we show that the *Toxoplasma* tachyzoite secretes toxofilin, which accelerates actin filament turnover and retrograde flow that in turn loosens the local host cell actin meshwork, facilitating parasite invasion.

We first found that parasites lacking toxofilin were impaired in cell invasion although they eventually entered host cells. Their internalization was significantly prolonged compared with the WT, with a substantial number displaying atypical behaviors, such as twisting and reorienting at sharp angles relative to the host cell. They were also occasionally observed to halt during their forward progression and pull the host cell plasma membrane around them. Moreover, the frequencies of these abnormal behaviors increased up to ~60% when host cells formed a monolayer, suggesting that the entry impediment of the toxofilin-KO tachyzoites was due to the host cortical actin constraints that

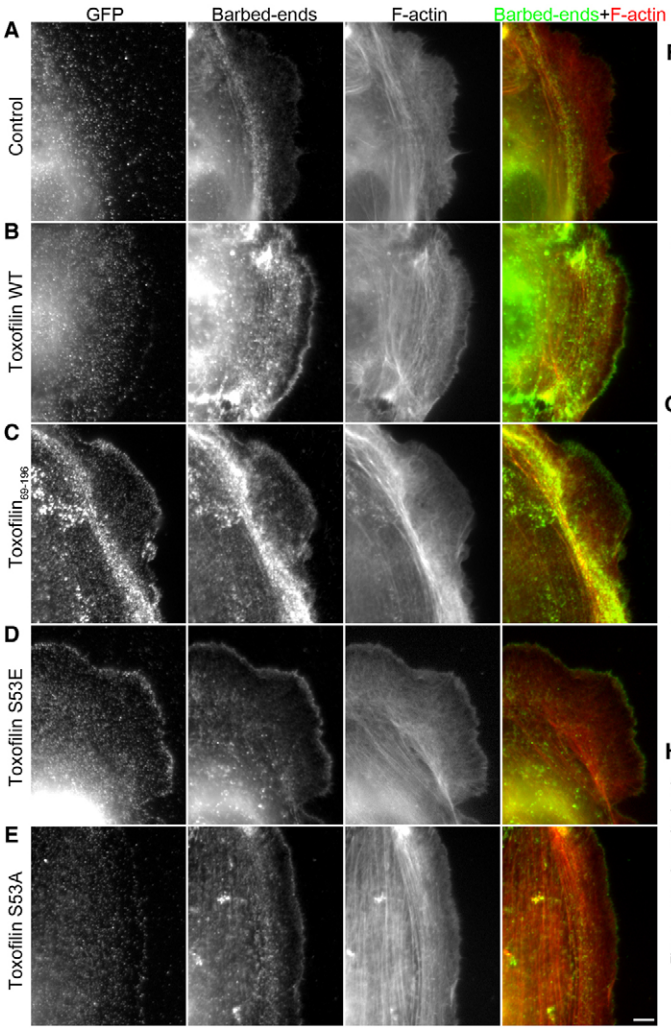

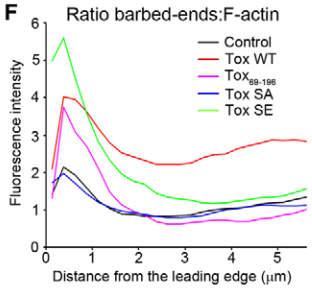

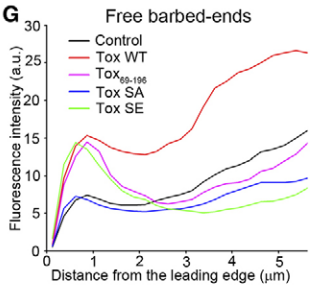

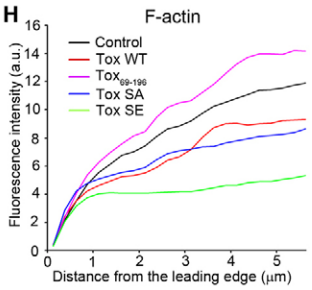

Fig. 8. Toxofilin increases the formation of polymerization-competent free barbed-ends. (**A-E**) Free barbed-end actin incorporation (green in merged image) and phalloidin staining (red in merged image) in PtK1 cells expressing GFP (A, noted control), GFP–toxofilin WT (B), GFP–toxofilin$_{69\text{-}196}$ (C), GFP–toxofilin S53E (D) or GFP–toxofilin S53A (E). Scale bar: 5 μm. (**F-H**) Fluorescence intensity of (F) free barbed-ends actin incorporation relative to F-actin, (G) free barbed-end actin incorporation, and (H) F-actin in control (black), toxofilin WT (red), toxofilin$_{69\text{-}196}$ (pink), toxofilin S53E (blue), toxofilin S53A (green), measured from the leading edge (0 μm) to the cell center (5 μm). The data shown are representative of one experiment and are the average from ≥9 cells for each condition. The experiment was repeated three times, with similar results.

zoites face before penetration. Toxofilin-KO tachyzoites indeed caused no detectable cortical actin disorganization, supporting the exclusive contribution of toxofilin in the process.

Recent work, using a reporter assay, has already described the secretion of toxofilin in the cytoplasm of host cells upon tachyzoite entry (Loeden et al., 2010). We showed that toxofilin localizes in the rhoptry bulb and in the distal duct, and is therefore ideally located for early secretion during cell entry. We also tracked toxofilin in action in the host cell through the combination of fluorescence and electron microscopy with electron tomography. This correlative assay offers the power of high-resolution and three-dimensional structural characterization of the parasite–host cell interactions at the site of entry. It revealed that the integrity of the host cortical actin cytoskeleton was disrupted at the site of parasite entry, suggesting that actin depolymerizes at the zoite apex before the forming PV. Furthermore, 3D immunogold labeling showed that toxofilin associated with the host cortical actin network. The limited amount of protein restricted to the site of entry appears fully compatible with an actin disassembling or severing activity working at sub-stoichiometric ratios with actin.

To then analyze how toxofilin controls actin dynamics at the cell edge, we used qFSM, a method that reveals the dynamics of protein assemblies and that has provided over the past decade detailed characterization of the turnover of actin filaments, microtubules and intermediate filaments in cells (Danuser and Waterman-Storer, 2006). We found that toxofilin accelerates actin filament turnover and retrograde flow reminiscent of the previously described activity of cofilin (Delorme et al., 2007), suggesting that toxofilin could sever actin filaments, in addition to its known activities of F-actin capping and monomer sequestering. Of note, using the actin free barbed-end assay we identified a pool of ectopically expressed toxofilin, which systematically localized at the cell leading edge, as already described for cofilin.

Toxoplasma tachyzoites thus appear to have selected their own host actin disassembly factor to rapidly disperse the cortical actin barrier and facilitate cell penetration. It might seem surprising that no ortholog has been found in other members of the phylum including *Plasmodium* species, which also need to pass through an actin cortical barrier to enter cells. However, it is possible that *Plasmodium* does not need cortical actin disrupting activity, since the merozoite stage invade red blood cells, which have a cortical spectrin/actin cytoskeleton, and the sporozoite stage invades hepatocytes, both of which are less bulky and more flexible than *Toxoplasma* tachyzoites. Alternatively, *Plasmodium* spp. might use a yet unidentified functional homolog of toxofilin during invasion. The tachyzoite needs to manipulate host cell dynamics

in apparently two opposing ways to enter the host cell: an actin 'depolymerization' activity to disrupt and pass through the cortical actin and an actin 'polymerization' activity to build the TJ through which it pulls to move inside the cell. It is tempting to speculate that the latter activity might feed off the former in a fast coupling event at the cell edge, as it is now well accepted during endocytosis in yeast (Okreglak and Drubin, 2010).

The importance of toxofilin to the tachyzoite within its host remains an open question. Although we have shown a clear contribution of toxofilin to the invasion process, which influences the duration of the process, tachyzoites devoid of toxofilin eventually invade host cells at normal levels *in vitro*. Could the rapidity of the invasion process confer a selective advantage to the parasite *in vivo*? Reactivation of the parasitic process that often leads to severe necrotic abscesses, in particular in the central and peripheral nervous tissues and muscles, implicates a massive tachyzoite production that relies on successful invasion. The rapidity of host cell invasion might represent a means of proteolytic and immune escape *in vivo*.

Materials and Methods

Cell and parasite culture

Rat mammary adenocarcinoma cells (MTLn3), normal rat kidney fibroblasts (NRK), human foreskin fibroblasts (HFF), human embryonic kidney cells (HEK293) and human epithelial cervical cancer cells (HeLa) were grown in Dulbecco's modified Eagle's medium (DMEM) supplemented with glutamax (Gibco), 10% heat-inactivated FCS, penicillin (100 IU/ml), streptomycin (100 mg/ml) and 10 mM HEPES, at 37℃ in a 5% CO_2 atmosphere. Rat kangaroo kidney epithelial cells (PtK1) were cultured in Ham's F12-medium (Sigma-Aldrich) containing 25 mM HEPES, 10% FBS and antibiotics. *T. gondii* RH strains (RH, RH–GFP, RH–GFPΔtoxofilin) were propagated on HFF cells as described previously (Roos et al., 1994).

Invasion/egress assays, evacuole assays and immunofluorescence

NRK or HFF cells were infected with tachyzoites for ~24 h. Cells were either fixed directly with 4% paraformaldehyde (PFA) in PBS, pH 7.5 (20 min, 23℃) or rinsed in warmed Hanks' balanced salt solution (HBSS; Gibco) and incubated for 20 seconds in the buffer containing 1 µM ionomycin (Sigma) to induce egress before fixation. Cells were incubated (1 h, 23℃) with either anti-toxofilin antibodies (1:500 dilution) or anti-Ron4 antibodies (1:200 dilution) followed by Alexa Fluor 488 anti-rabbit antibodies (1:1500 dilution; Molecular Probes) in PBS containing 2% BSA. Cells were then incubated with anti-Rop2-4 antibodies (1:100 dilution) followed by Alexa Fluor 546 anti-mouse antibodies (1:1500 dilution; Molecular Probes). Samples were mounted on slides in Mowiol 4-88 (Calbiochem). Images were obtained using a confocal laser microscope (TCS SP2 AOBS, Leica) and analyzed with ImageJ (W. Rasband, NIH, Bethesda, MD) or Adobe Photoshop softwares. In some experiments, tachyzoites were exposed to 1 µM jasplakinolide (Alexis; 30 min, 37℃). Evacuole assays were performed as described previously (Håkansson et al., 2001) in HFF cell monolayers infected with WT or toxofilin-KO tachyzoites expressing GFP. The parasite Rhop1 protein was detected using anti-Rhop1 antibodies (1:150 dilution) followed by Alexa Fluor 546 anti-mouse antibodies (1:1500 dilution; Molecular Probes). Evacuoles were identified as Rhop1-positive vesicular and tubular structures in the host cell in the vicinity of the attached parasite. One hundred attached parasites were scored in two separate experiments.

Cell transfection, co-immunoprecipitation and western blotting

HEK293 cells were transfected at ~70% confluency with 1 µg of vector encoding Myc–toxofilin full length alone or in combination with 1 µg of HA–cofilin construct using the Lipofectamine 2000 transfection reagent (Invitrogen). After ~24 h, cells were lysed in 50 mM Tris-HCl, pH 7.5, 150 mM NaCl, 0.1 mM $CaCl_2$, 0.05% Triton X-100 supplemented with protease inhibitors cocktail (Sigma; 20 min, 4℃). After centrifugation (20,000 ***g***, 15 min, 4℃), the supernatant was incubated with agarose beads (30 min, 4℃) then with anti-c-Myc–agarose affinity gel (Sigma; 2 h, 4℃). The resin was extensively washed, and bound proteins were eluted in SDS sample buffer. Proteins were separated by SDS-PAGE and transferred onto nitrocellulose membranes. Western blotting was performed using ECL+ as the detection system (GE) with anti-Myc (clone 9E10, 1:2000 dilution; Santa Cruz Biotechnology), polyclonal anti-HA (1:6000 dilution; Santa Cruz), anti-tubulin (clone DM 1A, 1:2000; Sigma), polyclonal anti-cofilin (1:1000 dilution; Cytoskeleton) or anti-actin (clone C4, 1:4000 dilution; Upstate) antibodies.

RNA interference and invasion assays

HeLa cells, grown at ~50% confluency, were transfected with or without 100 nM siRNA duplex targeting human cofilin and ADF or with siRNA that did not target a gene (siGFP; Eurogentec) and using Lipofectamine RNAi max (Invitrogen). Cells were plated 24 h later on poly-L-lysine-coated glass coverslips and incubated for 48 h in culture medium. At 72 h post-transfection, invasion assays were performed (Moi: 1:5; 1 h, 37℃, 5% CO_2). Cells were then fixed and stained for selective labeling of extracellular tachyzoites with anti-P30 antibodies and Hoechst staining. Intracellular tachyzoites were quantified in 300 cells, in triplicate (>5 independent experiments, a representative experiment is shown: NS, >0.05, Student's *t*-test) or by fluorescence-activated cell sorting using GFP-expressing parasite strains (n=50,000 cells per sample). The efficacy of cofilin silencing was analyzed on a whole cell population at 72 h post-transfection by SDS-PAGE and western blotting using anti-cofilin and anti-tubulin antibodies as detailed above. Membranes were scanned (Odyssey Li-Cor) and the cofilin signal was normalized using the loading control tubulin.

Videomicroscopy and time-lapse analysis

Time-lapse video microscopy was conducted as previously described (Gonzalez et al., 2009). Frames of zoites immediately before entry and precisely half way into the host cell were selected from the videomicroscopy stacks for both WT and toxofilin-KO samples (WT: n=29, KO: n=34). Using ImageJ, the constriction of each entering zoite was quantified by calculating the ratio of the largest width of the zoite measured before entry to the maximum width of the junction during invasion. Statistical analyses were performed using a Student's *t*-test.

Fluorescent speckle microscopy

Two days prior to experiments, PtK1 cells were plated on glass coverslips. Plasmids encoding GFP, GFP-tagged toxofilin WT, S53E, S53A or toxofilin$_{69\text{-}196}$ were injected into the nucleus (150 ng/µl). For fluorescent speckle microscopy (FSM) experiments, X-rhodamine-conjugated actin, was injected into cells at 0.8-1 mg/ml. Plasmids and fluorescent actin were co-injected into the cell nucleus. Live-cell microscopy was performed 3-6 h after injection: F-actin FSM and phase-contrast time-lapse image series were acquired at 5 sec intervals for 10 min on a spinning-disk confocal microscope with a CoolSnapHQ camera. F-actin flow rates at the cell leading edge were measured by kymograph analysis. Flow maps and F-actin polymerization/depolymerization maps were calculated using the fsmCenter software package written in Matlab (Mathworks) (Danuser and Waterman-Storer, 2006).

Correlative light and electron microscopy imaging

Ptk1 or NRK cells were grown on home-made holey carbon-coated 100 mesh finder grids and processed for electron microscopy. The invasion assay was stopped after 6 min by fixing cells in cytoskeleton buffer (10 mM MES, 3 mM $MgCl_2$, 138 mM KCl, 2 mM EGTA; pH 6.9) containing 4% paraformaldehyde (PFA) and blocked with 2% BSA in cytoskeleton buffer. Extracellular tachyzoites were then immunolabeled with anti-P30 monoclonal antibodies followed by incubation with Alexa Fluor 488 anti-mouse antibodies. For toxofilin immunogold labeling, cells were permeabilized in cytoskeleton buffer containing 0.2% Tween 20 (Thermo Scientific). Toxofilin was detected using anti-toxofilin rabbit polyclonal antibodies followed by incubation with Alexa-Fluor-488–10-nm-gold or 15-nm-gold anti-rabbit antibodies (Molecular Probes and BBInternational, respectively). Invading tachyzoites were identified by epifluorescence using an inverted microscope, and the same parasites were located in electron microscopy images by correlation with phase-contrast images (for example Fig. 2A,B). Electron microscopy images were obtained under low-dose conditions using a Tecnai G2 T12 microscope (FEI Company) equipped with a Lab6 filament (Denka) at 120 kV and recorded on Kodak ISO-163 plates (Eastman Kodak Co.).

Electron tomography and image analysis

The selected parasites were then subjected to dual-axis electron tomography. Dual-axis tilt series (approximately −70 to +70°, every 2°) were acquired on a Tecnai G2 F20 (FEI Company) equipped with an energy filter (zero-loss, Gatan Inc.) using a 2020 advanced tomography holder (Fishione Instruments). The data was collect using SerialEM. 3D reconstructions were generated using the IMOD package, and segmentation was achieved using the watershed algorithm (Volkmann, 2002). Surface representations and movies were generated using Chimera (Goddard et al., 2007).

Free barbed-end assay

To locate and quantify the density of actin polymerization-competent free barbed-ends, PtK1 cells were transfected with GFP empty vector (control), GFP-tagged toxofilin WT, S53E, S53A or toxofilin$_{69\text{-}196}$ using Lipofectamine LTX (Invitrogen). Live cells were permeabilized 16 h post-transfection with 0.25 mg/ml saponin in the presence of 0.5 µM X-rhodamine actin for 2 min, and fixed as previously described (Symons and Mitchison, 1991). F-actin was detected using Alexa-Fluor-350-conjugated phalloidin (Molecular Probes). Epifluorescence

images of fixed cells were acquired on an inverted microscope (Eclipse TE 2000-U, Nikon) equipped with an electronically controlled shutter, filter wheels, and a 14-bit cooled CCD camera (Cool SNAP HQ, Photometrics) controlled by MetaMorph software (Universal Imaging Corp.) with a 60×/1.4 NA Plan Apo DIC objective lens (Nikon). Quantification of the fluorescence of free barbed-ends and F-actin as a function of the distance from the cell edge was obtained with custom software written in Matlab (MathWorks).

Acknowledgements

We are deeply grateful to the late Professor Gary M. Bokoch (Department of Immunology and Microbial Science, The Scripps Research Institute, La Jolla, CA 92037, USA) who welcomed V. D-W. to his laboratory and funded her there. We thank Robert Ménard for critical input into the manuscript. We thank John Boothroyd and Melissa Lodoen for their gift of the toxofilin-KO and WT RH *Toxplasma* strains, and Gary Ward and Maryse Lebrun for providing us with anti-AMA1 and anti-Ron4 antibodies, respectively. We thank the Cochin Institute Imaging facility for access to the center for image acquisition.

Funding

This work was supported by the Centre National de la Recherche Scientifique (CNRS) starting grant (ATIP-MIE) and the French government research agency [grant number ANR-MIERPV08023KSA to I.T.]; the European SP7 cooperation [grant number MALSIG 223044 to I.T..]; the National Institute of General Medical Sciences Cell Migration Consortium (for the correlative light and electron microscopy studies) [grant numbers U54 GM064346 and P01 GM098412 to D.H. and N.V.]; the Fondation pour la Recherche Medicale PhD fellowship to V.D-W.; and the American Heart Association [grant numbers 0525040Y and 0825165F to V.D-W.]. Deposited in PMC for release after 12 months.

Supplementary material available online at
http://jcs.biologists.org/lookup/suppl/doi:10.1242/jcs.103648/-/DC1

References

Alexander, D. L., Mital, J., Ward, G. E., Bradley, P. and Boothroyd, J. C. (2005). Identification of the moving junction complex of *Toxoplasma gondii*: a collaboration between distinct secretory organelles. *PLoS Pathog.* **1**, e17.

Besteiro, S., Michelin, A., Poncet, J., Dubremetz, J. F. and Lebrun, M. (2009). Export of a *Toxoplasma gondii* rhoptry neck protein complex at the host cell membrane to form the moving junction during invasion. *PLoS Pathog.* **5**, e1000309.

Bradley, P. J. and Sibley, L. D. (2007). Rhoptries: an arsenal of secreted virulence factors. *Curr. Opin. Microbiol.* **10**, 582-587.

Bradley, P. J., Ward, C., Cheng, S. J., Alexander, D. L., Coller, S., Coombs, G. H., Dunn, J. D., Ferguson, D. J., Sanderson, S. J., Wastling, J. M. et al. (2005). Proteomic analysis of rhoptry organelles reveals many novel constituents for host-parasite interactions in *Toxoplasma gondii*. *J. Biol. Chem.* **280**, 34245-34258.

Danuser, G. and Waterman-Storer, C. M. (2006). Quantitative fluorescent speckle microscopy of cytoskeleton dynamics. *Annu. Rev. Biophys. Biomol. Struct.* **35**, 361-387.

Delorme, V., Cayla, X., Faure, G., Garcia, A. and Tardieux, I. (2003). Actin dynamics is controlled by a casein kinase II and phosphatase 2C interplay on *Toxoplasma gondii* Toxofilin. *Mol. Biol. Cell* **14**, 1900-1912.

Delorme, V., Machacek, M., DerMardirossian, C., Anderson, K. L., Wittmann, T., Hanein, D., Waterman-Storer, C. M., Danuser, G. and Bokoch, G. M. (2007). Cofilin activity downstream of Pak1 regulates cell protrusion efficiency by organizing lamellipodium and lamella actin networks. *Dev. Cell* **13**, 646-662.

Dobrowolski, J. M. and Sibley, L. D. (1996). *Toxoplasma* invasion of mammalian cells is powered by the actin cytoskeleton of the parasite. *Cell* **84**, 933-939.

Goddard, T. D., Huang, C. C. and Ferrin, T. E. (2007). Visualizing density maps with UCSF Chimera. *J. Struct. Biol.* **157**, 281-287.

Gonzalez, V., Combe, A., David, V., Malmquist, N. A., Delorme, V., Leroy, C., Blazquez, S., Ménard, R. and Tardieux, I. (2009). Host cell entry by apicomplexa parasites requires actin polymerization in the host cell. *Cell Host Microbe* **5**, 259-272.

Gupton, S. L., Anderson, K. L., Kole, T. P., Fischer, R. S., Ponti, A., Hitchcock-DeGregori, S. E., Danuser, G., Fowler, V. M., Wirtz, D., Hanein, D. et al. (2005). Cell migration without a lamellipodium: translation of actin dynamics into cell movement mediated by tropomyosin. *J. Cell Biol.* **168**, 619-631.

Håkansson, S., Charron, A. J. and Sibley, L. D. (2001). Toxoplasma evacuoles: a two-step process of secretion and fusion forms the parasitophorous vacuole. *EMBO J.* **20**, 3132-3144.

Hanein, D. (2010). Tomography of actin cytoskeletal networks. *Methods Enzymol.* **483**, 203-214.

Jan, G., Delorme, V., David, V., Revenu, C., Rebollo, A., Cayla, X. and Tardieux, I. (2007). The toxofilin-actin-PP2C complex of *Toxoplasma*: identification of interacting domains. *Biochem. J.* **401**, 711-719.

Lee, S. H., Hayes, D. B., Rebowski, G., Tardieux, I. and Dominguez, R. (2007). Toxofilin from *Toxoplasma gondii* forms a ternary complex with an antiparallel actin dimer. *Proc. Natl. Acad. Sci. USA* **104**, 16122-16127.

Lodoen, M. B., Gerke, C. and Boothroyd, J. C. (2010). A highly sensitive FRET-based approach reveals secretion of the actin-binding protein toxofilin during *Toxoplasma gondii* infection. *Cell. Microbiol.* **12**, 55-66.

Meissner, M., Schlüter, D. and Soldati, D. (2002). Role of *Toxoplasma gondii* myosin A in powering parasite gliding and host cell invasion. *Science* **298**, 837-840.

Mordue, D. G., Desai, N., Dustin, M. and Sibley, L. D. (1999). Invasion by *Toxoplasma gondii* establishes a moving junction that selectively excludes host cell plasma membrane proteins on the basis of their membrane anchoring. *J. Exp. Med.* **190**, 1783-1792.

Okreglak, V. and Drubin, D. G. (2010). Loss of Aip1 reveals a role in maintaining the actin monomer pool and an in vivo oligomer assembly pathway. *J. Cell Biol.* **188**, 769-777.

Ono, S. (2003). Regulation of actin filament dynamics by actin depolymerizing factor/cofilin and actin-interacting protein 1: new blades for twisted filaments. *Biochemistry* **42**, 13363-13370.

Ponti, A., Machacek, M., Gupton, S. L., Waterman-Storer, C. M. and Danuser, G. (2004). Two distinct actin networks drive the protrusion of migrating cells. *Science* **305**, 1782-1786.

Poupel, O., Boleti, H., Axisa, S., Couture-Tosi, E. and Tardieux, I. (2000). Toxofilin, a novel actin-binding protein from *Toxoplasma gondii*, sequesters actin monomers and caps actin filaments. *Mol. Biol. Cell* **11**, 355-368.

Rodal, A. A., Tetreault, J. W., Lappalainen, P., Drubin, D. G. and Amberg, D. C. (1999). Aip1p interacts with cofilin to disassemble actin filaments. *J. Cell Biol.* **145**, 1251-1264.

Roos, D. S., Donald, R. G., Morrissette, N. S. and Moulton, A. L. (1994). Molecular tools for genetic dissection of the protozoan parasite *Toxoplasma gondii*. *Methods Cell Biol.* **45**, 27-63.

Shaw, M. K. and Tilney, L. G. (1999). Induction of an acrosomal process in *Toxoplasma gondii*: visualization of actin filaments in a protozoan parasite. *Proc. Natl. Acad. Sci. USA* **96**, 9095-9099.

Straub, K. W., Cheng, S. J., Sohn, C. S. and Bradley, P. J. (2009). Novel components of the Apicomplexan moving junction reveal conserved and coccidia-restricted elements. *Cell. Microbiol.* **11**, 590-603.

Suss-Toby, E., Zimmerberg, J. and Ward, G. E. (1996). *Toxoplasma* invasion: the parasitophorous vacuole is formed from host cell plasma membrane and pinches off via a fission pore. *Proc. Natl. Acad. Sci. USA* **93**, 8413-8418.

Symons, M. H. and Mitchison, T. J. (1991). Control of actin polymerization in live and permeabilized fibroblasts. *J. Cell Biol.* **114**, 503-513.

Tran Van Nhieu, G., Bourdet-Sicard, R., Duménil, G., Blocker, A. and Sansonetti, P. J. (2000). Bacterial signals and cell responses during Shigella entry into epithelial cells. *Cell. Microbiol.* **2**, 187-193.

Vallance, B. A. and Finlay, B. B. (2000). Exploitation of host cells by enteropathogenic Escherichia coli. *Proc. Natl. Acad. Sci. USA* **97**, 8799-8806.

Volkmann, N. (2002). A novel three-dimensional variant of the watershed transform for segmentation of electron density maps. *J. Struct. Biol.* **138**, 123-129.

Waterman-Storer, C. M., Desai, A., Bulinski, J. C. and Salmon, E. D. (1998). Fluorescent speckle microscopy, a method to visualize the dynamics of protein assemblies in living cells. *Curr. Biol.* **8**, 1227-1230.

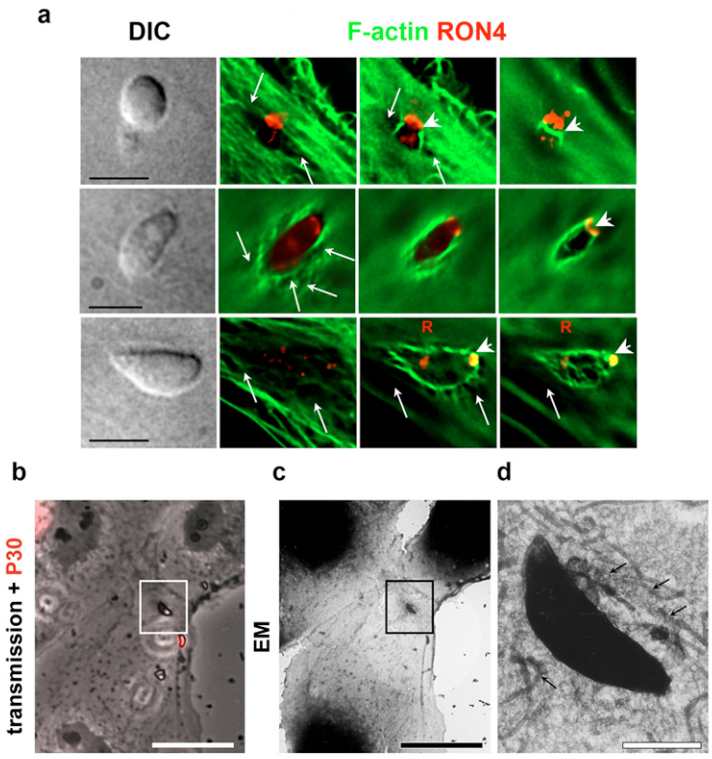

Fig. S1. Fluorescence microscopy and correlative fluorescence and transmission electron microscopy of invading and internalized tachyzoites in Ptk1 cells. (**A**) Confocal microscopy of host cell F-actin (green) at the site of entering parasites for 3 different planes. The RON4 labeling (red) delineates the zoite-cell junction (white arrowhead) and stains the rhoptries. Scale bar, 5 mm. (**B**) Overlay of P30 fluorescence image (red) and a phase contrast image. Scale bar, 30 mm. (**C**) Transmission electron micrograph of the same field of view as shown in b. (**D**) High resolution electron micrograph of fully-internalized tachyzoite identified by the absence of P30 fluorescence in b. Scale bar, 2 mm. Black arrows indicate the accumulation of endoplasmic reticulum in the vicinity of the parasite.

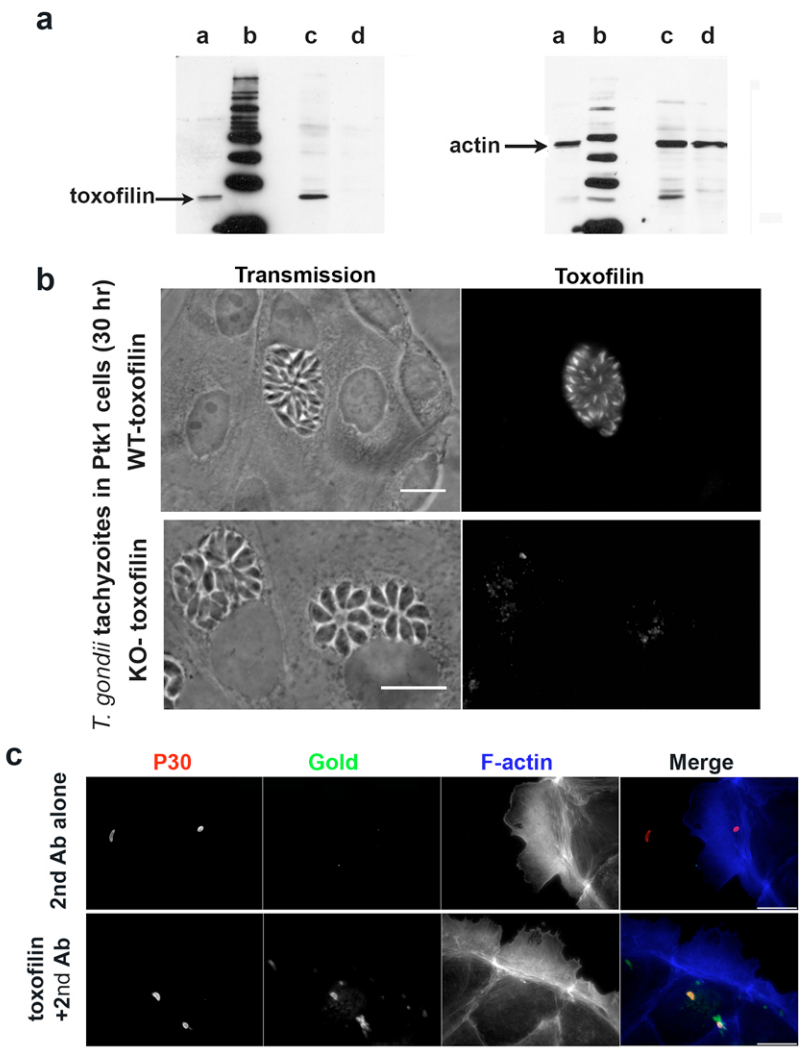

Fig. S2. Toxofilin signals visualized by immunofluorescence and immunogold microscopy are specific. (A) Western blot of total extract of free WT-toxofilin tachyzoites (10^6) (lane a) and HFF cells (~2×10^5) infected with WT-toxofilin (lane c) and KO toxofilin (lane d) tachyzoites; lane b presents the molecular weight markers. The membrane was probed first using the anti-toxofilin antibodies (left panel) and then anti-Tg actin antibodies (right panel) **(B,C)** Invasion assay was performed on PtK1 cells. (B) Toxofilin was detected using anti-toxofilin antibodies followed by Alexa Fluor 488. Scale bar, 10 mm. (C) Cells were prepared as for immunogold EM experiment. Extracellular tachyzoites were detected using anti-P30 antibodies and Alexa Fluor 568 anti-mouse secondary antibodies (shown in red in the merge column). Toxofilin was detected using anti-toxofilin antibodies followed by Alexa Fluor 488-15 nm gold anti-rabbit antibodies (shown in green in the merge column). In control, secondary Alexa Fluor 488-15 nm gold anti-rabbit antibodies were used alone without anti-toxofilin. F-actin was visualized with Alexa Fluor 350-phalloidin. Scale bar, 20 mm.

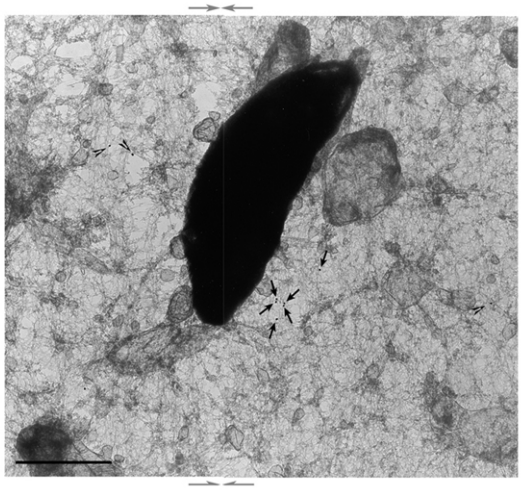

Fig. S3. A larger field of view than that the one presented in Fig. 3A-E showing gold labeling of toxofilin at the onset of Ptk1 cell invasion by a tachyzoite. The figure is reconstituted from 2 separate electron microscopy micrographs (see grey arrows at the edge of the figure) and shows that toxofilin secretion is specifically localized in the vicinity of the parasite. Scale bar, 1 mm. The view is rotated by 20° counterclockwise from the view in Fig. 3A,B. The arrows point to the gold labels depicted in Fig. 3A-E. The three additional black arrowheads point to gold labels outside the field of view shown in Fig. 3.

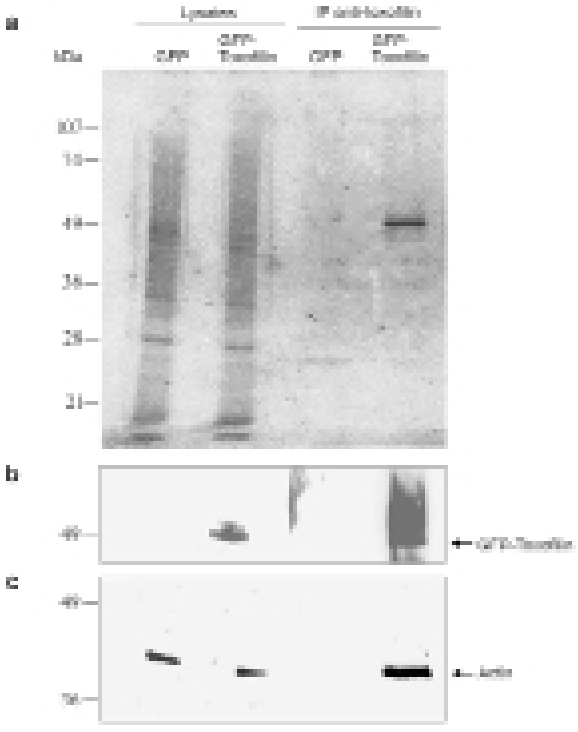

Fig. S4. Toxofilin is phosphorylated when expressed in cells. HeLa cells were transfected with GFP alone or GFP-toxofilin and labeled with ^{32}P. Toxofilin was immunoprecipitated from cell lysates. (**A**) Radioactive scan of whole cell lysates and immunopreciptation eluates. (**B**) Western blot using anti-Toxofilin. (**C**) Western-blot using anti-actin.

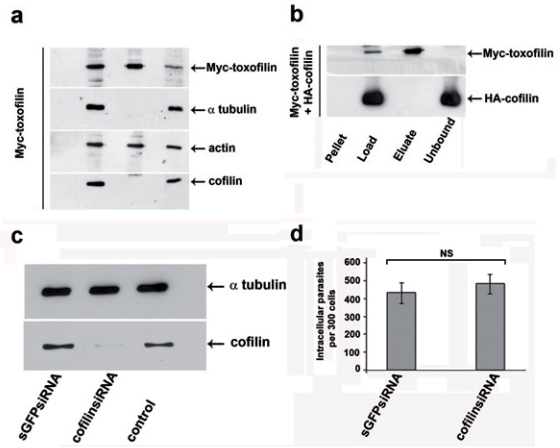

Fig. S5. Toxofilin upregulates actin turnover independently of host cell cofilin. HEK293 cells were transfected with myc-toxofilin **(A)**, or with both myc-toxofilin and HA-cofilin **(B)** to detect putative partners. Lysates were subjected to immunoprecipitation using anti-myc antibodies. (A) Immunoprecipitation of toxofilin does not pull down endogenous cofilin, nor tubulin, but co-purifies with actin as expected. (B) Ectopically expressed HA-cofilin is not co-precipitating with myc-toxofilin. **(C)** HeLa cells were specifically silenced for cofilin as controlled using western blot, and **(D)** invasion assays were performed on control and silenced cells: no significant differences were observed in the number of infected cells (P>0.05, Student t-test).